Selective disordering of lamella-forming diblock copolymers under an electric field

ARTICLE *in* SOFT MATTER · MAY 2011

Impact Factor: 4.03 · DOI: 10.1039/c0sm01395a

4 AUTHORS:

Geert J A Sevink
Leiden University
78 PUBLICATIONS **2,393** CITATIONS
SEE PROFILE

Marco Pinna
University of Lincoln
31 PUBLICATIONS **234** CITATIONS
SEE PROFILE

Karol M. Langner
Google Inc.
17 PUBLICATIONS **1,174** CITATIONS
SEE PROFILE

Andrei V Zvelindovsky
University of Lincoln
114 PUBLICATIONS **2,418** CITATIONS
SEE PROFILE

Soft Matter

View Online
Dynamic Article Links

Cite this: *Soft Matter*, 2011, **7**, 5161

www.rsc.org/softmatter

PAPER

Selective disordering of lamella-forming diblock copolymers under an electric field

G. J. A. Sevink,*[a] M. Pinna,[b] K. M. Langner[a] and A. V. Zvelindovsky*[b]

Received 30th November 2010, Accepted 15th April 2011
DOI: 10.1039/c0sm01395a

Self-assembled block polymers show great potential to serve as templates for the fabrication of nanoscale structures for devices, provided that structural features such as defects and global orientation can be fully and efficiently controlled. The most efficient way to control these features is by application of an electric field, to orient features parallel to the electric field. Several aspects of the thermodynamic and kinetic factors that determine the reorientation dynamics have been studied in recent years and are increasingly understood. Current experiments focus on reorientation close to the order-disorder transition (ODT) temperature, where an efficient mechanism involving selective disordering is long anticipated but subject to lively debate. Here, we complement the increasing experimental understanding by a detailed and unifying computational analysis of all distinct microscopic stages in this new reorientation mechanism. The unification step originates from the comparison of two different models, one based on a molecular description and the other phenomenological. The results have a general character and may also serve as a stepping stone for understanding microscopic response pathways due to other kinds of deformation, such as mechanical stress or shear. We find that reorientation is most effective for temperatures that are slightly below ODT, at which the system is slightly demixed and the balance between surface tension and the ponderomotive force is optimal.

1 Introduction

Electric-field-induced manipulation is considered the most efficient method for tailoring oriented and neat structures in soft nanotechnology from block copolymers.[1,2] The experimental features of this complex phenomenon were extensively studied over the last fifteen years.[3–8] Theoretically, the focus has been on deriving a static collection of phase diagrams using either Ginsburg–Landau (GL) free energy expressions[9] or self-consistent field theory (SCFT)[10–12] for various systems or the shift of the order-disorder transition (ODT) temperature due to an applied electric field.[13,14] Reorientation kinetics, in lamellar nanostructures, has primarily been considered using linear stability analysis, by either the GL approach[15] or SCFT,[10,16] and by considering the dynamics of an undulation instability.[17] Although these treatments are applicable at the onset of an instability, they are in general insufficient for the understanding of complete reorientation pathways that are observed in experiments, which are intricate nonlinear phenomena. In addition, including the experimental imperfection and defects in a transition state treatment based on SCFT in Fourier space currently represents a too formidable task.[16]

Böker and coworkers experimentally identified two distinct mechanisms for the electric-field-induced alignment of diblock copolymer lamellae using X-ray scattering.[18] They showed that close to ODT the scattering peak of lamellae parallel to the electrodes quickly disappears and a new peak emerges, originating from lamellae aligned with the electric field. Further from ODT, the peak merely rotates from its initial position towards the final one. The authors argued[18] that the two mechanisms are distinguished due to kinetic factors, such as different initial grain size, mobility, and viscosity. Using dynamic density functional theory (DDFT), based on a microscopic Hamiltonian for ideal Gaussian chains with mean field interactions that is essentially the same as considered in SCFT, we have previously showed[19] that this experimental behaviour can be explained in terms of a thermodynamic factor only. In particular, the alignment mechanisms are discriminated by energetics, namely, by the balance of the ponderomotive force (controlled by the field strength) and the strength of the interface (controlled by the Flory–Huggins χ parameter). Two microscopic mechanisms were identified, *nucleation and growth* closer to ODT (A) and *rotation via* defect annihilation further from ODT (B). Closer examination by transmission electron microscopy (TEM) of arrested structure for the experimental mechanism close to ODT[20] revealed defect structures (undulating lamellae and pointlike microdomains) that closely resemble the computed intermediates for mechanism A.[19] A far reaching consequence of this finding is that the microscopic

[a]*Leiden Institute of Chemistry, Leiden University, PO Box 9502, 2300 RA Leiden, The Netherlands*
[b]*Computational Physics Group, University of Central Lancashire, Preston, PR1 2HE, United Kingdom*

reorientation mechanism for a block copolymer is completely determined by the distance to ODT, which can be controlled in experiments by either thermodynamic (temperature) or kinetic (polymer concentration) system properties.

Very close to ODT, the two opposite effects of an applied electric field, *i.e.* favored mixing and the suppression of composition fluctuations, may become comparable and lead to very complex behavior. Recently, cell dynamics simulations (CDS), based on a phenomenological GL Hamiltonian, revealed the existence of a third mechanism of *selective disordering* (A′) in this regime.[21] DeRouchey *et al.* concluded that selective disordering was also observed during the reorientation of a polystyrene-polyisoprene system, using small-angle X-ray scattering.[22] In addition, *complete* disordering was recently considered experimentally, in much more detail than before, and led to the identification of an unexpected asymmetry in the ODT dependence on the electric field strength E_0. With increasing E_0, the ODT decreases upon heating from the ordered to the disordered state, while the ODT is rather independent of E_0 upon cooling from the disordered to the ordered state.[23] The origin and fundamentals of this (asymmetric) disordering phenomenon remain unclear, as theoretical studies so far only agree that the effect should be more pronounced for increasing E_0.[3,13,24] Selective disordering was previously proposed as a mechanism for electric field alignment for very strong electric fields ($E_0 \sim 50$ V/μm), based on an estimate of the ODT difference between perfectly parallel and perpendicular lamellar alignments.[3] Nevertheless, the selective disordering mechanism A′ in Pinna *et al.*[21] was found already for much lower E_0, well within the accessible experimental range, indicating that Amundson's theoretical estimates for the threshold E_0-value for (partial) mixing derived from static theory may be too high. Alternatively, some argued that CDS is insufficient to capture the complexity of this phenomenon and suggested that mechanism A′ is observed as a result of numerical artifacts.

The purpose of this work is to reconsider mechanism A′ *via* a direct mapping between the CDS and earlier validated DDFT methods[19] for a lamella-forming system very close to ODT. Using this mapping, we will in more detail than before[21] analyze all microscopic features of the selective disordering pathway A′. By combining these and previous computational results further away from ODT,[19] for which DDFT contains a more appropriate free energy expression than CDS, we can determine the mean-field interaction parameter χ associated with the smallest characteristic reorientation time, *i.e.* identify the optimal reorientation process that is important for soft nanotechnology. Universality is suggested by the recognition of Amundson *et al.*,[3] that the electric field contribution to the free energy is similar in form to the one for mechanical deformation. As a result, these computational results may be representative for a whole class of stress-induced transitions, clearly showing the significance of the present work in a much broader context.

2 Method

A symmetric AB diblock copolymer can be described by a single order parameter $\psi(\mathbf{r}, t) = \phi_A - \phi_A{}^0$, where ϕ_A and $\phi_A{}^0$ are the local volume fractions of A monomers and their average value, respectively. The time evolution of $\psi(\mathbf{r}, t)$ is given by the Cahn–Hilliard–Cook or time-dependent Ginzburg–Landau equation, which in the presence of an electric field in the y-direction includes non-isotropic diffusion,[19,25,26]

$$\frac{\partial \psi}{\partial t} = M\left[\nabla^2\left(\frac{\delta F_0[\psi]}{\delta \psi}\right) + \tilde{\alpha}\nabla_y^2\psi\right], \quad (1)$$

where $\tilde{\alpha} = E_0^2\varepsilon_1^2\nu/(4\pi k_B T\bar{\varepsilon})$, M is a mobility, E_0 denotes the strength of the applied electric field and ν is the volume of a single polymer chain. We assumed linear dependence of the dielectric permittivity on the composition $\varepsilon(\mathbf{r}) = \bar{\varepsilon} + \varepsilon_1\psi(\mathbf{r})$,[12] in particular, $\bar{\varepsilon} = \varepsilon_0(\kappa_A + \kappa_B)/2$ and $\varepsilon_1 = \varepsilon_0(\kappa_A - \kappa_B)$, with ε_0 the vacuum permittivity and κ_A and κ_B the dielectric constant of pure A and B blocks. The last term in (1) is an analytic result based upon a linear expansion of the electrostatic free energy $F_E = -(1/2)\int_V \varepsilon(\mathbf{r})E(\mathbf{r})^2 d\mathbf{r}$, together with $\mathbf{E} = \mathbf{E}_0 - \nabla\varphi$ and Maxwell's equation $\nabla\cdot(\varepsilon(\mathbf{r})\mathbf{E}(\mathbf{r})) = 0$.[26] Here, we checked the approximation in eqn (1) by numerically solving the Maxwell equation instead. The details are given below. We have previously showed that for experimentally relevant block copolymers the considered $\tilde{\alpha} = 0.2$ yields a field strength of $E_0 \approx 10$ V/μm.[26]

Two already mentioned models for the non-electrostatic part of the free energy F_0 in eqn (1) are employed here, namely the phenomenological GL type,[21] and a microscopic description of Gaussian A_4B_4 chains in a mean-field environment (DDFT).[19,26] A two-dimensional system not far from ODT is studied, with a Flory–Huggins parameter of $\chi_{AB}N = 14$ (CDS).[21] The equivalent interaction parameter ε_{AB} in DDFT can be readily determined from $\chi_{AB}N$, but it is validated by direct mapping instead. In order to ensure similar starting conditions, this procedure always started from a self-organized structure for $\varepsilon_{AB} = 4.5$ (in kJ/mol[26]) after 10^4 steps. First, this structure was equilibrated during 2×10^3 time steps for a different, increased ε_{AB}. After equilibration, we reset the time to $t = 0$ and applied the electric field. We calculate the orientational order parameter that was also used in previous studies[18]

$$P_2(t) = \frac{3\langle cos^2\phi(t)\rangle - 1}{2}, \quad (2)$$

with

$$\langle cos^2\phi(t)\rangle = \frac{\int_0^{2\pi} d\phi\left(I_q(\phi)\cos^2(\phi)|\sin(\phi)|\right)}{\int_0^{2\pi} d\phi\left(I_q(\phi)|\sin(\phi)|\right)} \quad (3)$$

where $I_q(\phi)$ is the intensity on the first scattering ring obtained by a Fast Fourier Transform (FFT), to compare the electric field response to the CDS system. We found an adequate match for $\varepsilon_{AB} = 4.6$ or $\chi_{AB}N = 14.7$ (DDFT), as illustrated by the plot of $P_2(t)$ in Fig. 1c. Fig. 1a (CDS) and b (DDFT) show the evolution of scattering intensity $I(\phi)$. After the EF is turned on, the initial peaks at random angles disappear. From $t \approx 50$ onwards, peaks arise at $\phi = 90^0$ and 270^0 and grow in amplitude. Selective disordering manifests itself in the drastic initial drop of the integrated scattering intensity $\int I(\phi)d\phi$ in Fig. 1d.

We verify our model in eqn (1) by comparing it with a direct numerical solution of Maxwell equations. The results are presented in Fig. 2. It shows that the time evolution of the scattering intensity and the non-electrostatic part of the free energy F_0 agree

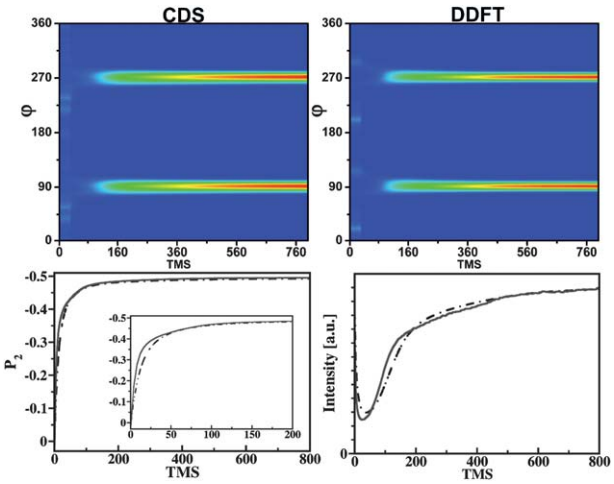

Fig. 1 Top: evolution of the scattering intensity $I(\phi)$ in the presence of an electric field as a function of number of time steps (TMS) in the CDS calculations, with CDS at the left and DDFT on the right. We used constant scaling to compensate for the different time increments in DDFT (0.2) and CDS (1). Here, ϕ is the azimuthal angle on the first scattering ring (for details see Böker *et al.*[18]). For clarity, $I(\phi)$ is repeated 10 times for the initial structure at $t = 0$. Bottom: the orientational order parameter P_2 and integrated scattering intensity $\int I(\phi)d\phi$ as a function of the time step (CDS - dashed line, DDFT - solid line). The inset shows P_2 in the early stages of the simulation.

very well in both approaches. The non-electrostatic part of the free energy is affected *via* changes in the structure due to the EF and can thus serve as an indicator of overall changes in the system.[26] In addition, we found that the microscopic pathway of reorientation dynamics was only marginally affected.

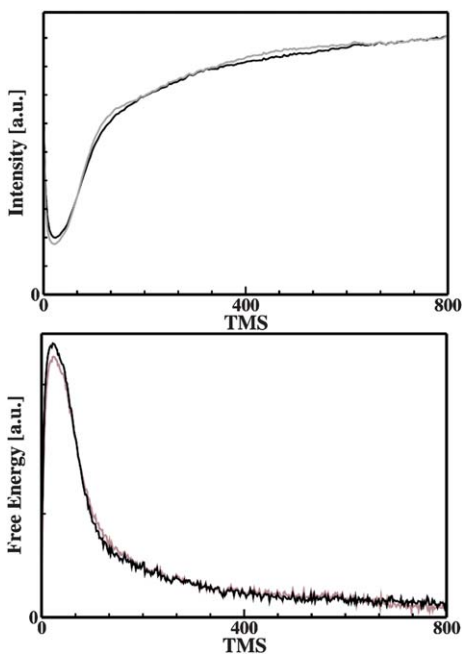

Fig. 2 Evolution of the scattering intensity $I(\phi)$ (top) and free energy F_0 (bottom) as a function of number of time steps (TMS) for DDFT calculations. Black lines correspond to the full solution of the Maxwell equations, while grey lines correspond to the expansion model in eqn (1).

3 Results and discussion

Fig. 3 shows four typical stages of lamellar reorientation *via* selective disordering obtained by the DDFT and CDS calculations. Color images depict the angle of the local microstructure relative to the electric field (EF) at the equivalent stages, using a procedure adopted from Berry *et al.*[27] that includes an additional constant threshold for the removal of (almost) vanishing gradients associated with regions where the order parameter $\psi \approx 0$. The initial structures (top row) are isotropic on a large scale and consist of multiple lamellar clusters with various orientations (colors), interconnected *via* characteristic defects and grain boundaries. Although they may not fully coincide due to differences in preparation history, we find that the studied pathway is sensitive only to the segregation regimes the systems are in.

After applying the electric field at $t = 0$, clusters exhibiting small angles to the EF direction (red and blue) survive, whereas clusters with larger angles (green/yellow) rapidly disappear (see $t = 20$). The decay rate depends on initial cluster orientation (color), indicating that selective disordering depends on the initial angle with respect to the EF. Clusters perpendicular to the EF (green) dissolve first, since the ponderomotive force is maximal for them, which agrees with a previous theoretical prediction by Onuki and Fukuda.[15]

Disordering proceeds *via* a decrease in the overall amplitude of lamellae and by the growth of undulations. While the surviving clusters grow in the field direction, new clusters nucleate in disordered regions (the black area in Fig. 3, $t = 60$). The new clusters exhibit increased growth rates in the direction perpendicular to the EF, leading to characteristic, elongated clusters. Such elongated, embryonic lamellar grains, embedded in a disordered matrix, have been observed with transmission electron microscopy at the onset of the ordered state.[28] With time, clusters eventually merge at grain boundaries, accompanied by local (transient) disordering and nucleation of new seeds in places where two lamellae are misaligned. The remaining individual defects migrate on a larger scale and annihilate by merging with oppositely charged defects.

3.1 Quantitative analysis

Minkowski functionals, calculated using a standard algorithm (see, for more details, ref. 1, Chapter 9), provide a quantitative way to analyze these transitions. The almost 60% decrease in lamellar cluster area between time steps 8–100 (Fig. 4) provides a direct confirmation of the selective disordering mechanism in both models. Nontrivial features of the kinetic pathway can be deducted from the evolution of the perimeter of lamellar clusters. For example, an initial increase in the perimeter corresponds to the system breaking into several lamellar clusters soon after applying the field. The dip that follows reflects the selective disordering (melting) of lamellar clusters perpendicular to the field. New and existing nuclei aligned with the electric field start to grow, which is seen by the second peak in the perimeter around a time step of 100, and the merging of multiple clusters reduces the total perimeter in the final stages.

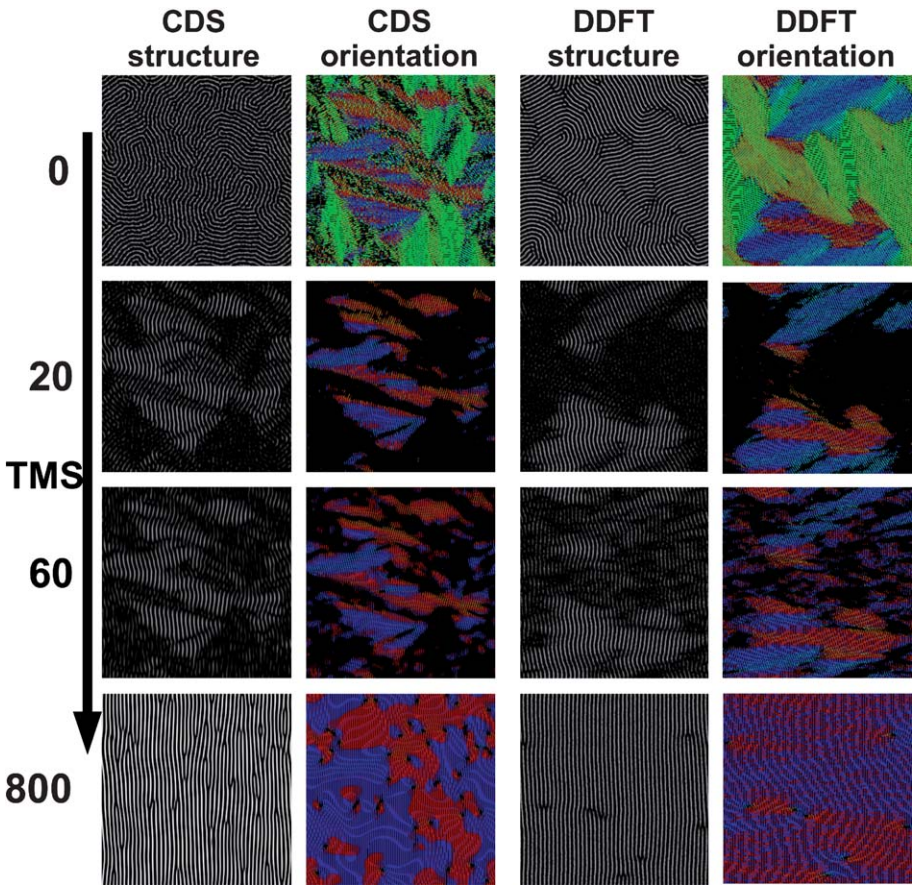

Fig. 3 Distinct stages of the reorientation pathway in terms of structure (b/w) and orientation (color) under an electric field ($\tilde{\alpha} = 0.2$). The stages are denoted by the corresponding $t =$ TMS in the CDS calculations. CDS: simulation box was 364×364, with all parameters the same as in our previous report,[21] except for the AB block interaction parameter $\tau = 0.30$. DDFT: simulation box was 256×256, with all parameters the same as previously,[19] except for the AB block interaction parameter $\varepsilon_{AB} = 4.6$. The color scheme, ranging from red (0°) to blue (180°), represents the angle ϕ relative to the electric field ($\Delta\phi = 1°$).

The Euler characteristic χ allows us to elaborate further on the shapes and topologies of clusters. The initial stage in Fig. 4 has two distinct regimes, the first exhibiting a decrease in χ to more negative values, indicating highly connected structures. This is followed by a steep increase to positive values, reflecting in turn the disassembly of connections and breaking up into separated lamellar clusters. The growth of newly formed nuclei eventually gives rise to merging and to the formation of new defects at grain boundaries, which corresponds to another drop in χ, back to negative values. Defect healing by local disassembly in the final stages is reflected in χ approaching zero, which would be the value for defect-free, parallel lamellae.

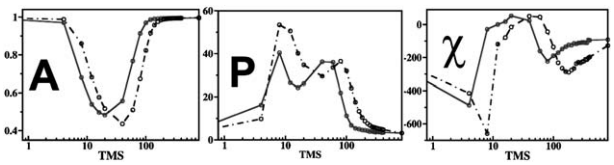

Fig. 4 Evolution of the Minkowski functionals as a function of TMS; A - area, P - perimeter, χ - Euler characteristic. (CDS - dashed line, DDFT - solid line.)

3.2 Characteristic reorientation times

To further evaluate kinetics, we consider in Fig. 5 the characteristic reorientation time τ as a function of $\varepsilon_{AB}(\sim \chi_{AB})$, which is inversely related to temperature. We used the data obtained by the mapping procedure that was described in the Method section.

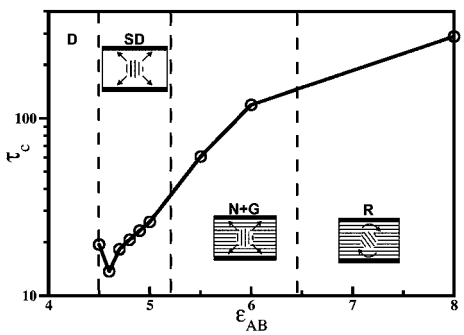

Fig. 5 Characteristic reorientation time τ determined by fitting a single exponential to $P_2(t)$ for varying interaction parameter ε_{AB} in DDFT. The dashed lines indicate estimated region boundaries, and the cartoons illustrate: disordered state (D), selective disordering (SD), nucleation and growth (N + G) and rotation by defect movement (R).

Deriving the value of τ by fitting $P_2(t)$ (see, for instance, Fig. 1) with a single exponential,[18]

$$P_{2,\,t} = P_{2,\,\infty} + (P_{2,\,0} - P_{2,\,\infty}) \exp(-t/\tau) \quad (4)$$

we find that τ is a non-monotonic function of ε_{AB} with a minimum value for $\varepsilon_{AB} = 4.6$. In spite of the same mechanism A′, applying an EF is apparently less effective in reorienting lamellae at $\varepsilon_{AB} = 4.5$ (higher temperature), which is the lowest value providing a well-defined structure because of the second order nature of ODT and finite calculation times. Since the only difference is in the degree of demixing, we conclude that a reduced ponderomotive force is the key to this effect.

3.3 Discussion

We conclude from the comparison that the two free energy expressions, the phenomenological GL type and the DDFT, can be exchanged rather freely for the considered χN range. We further concentrate on DDFT. Previous reports have shown that the diffusive model applied here provides an accurate dynamic description for a particular concentrated block copolymer.[29,30] Since the DDFT calculations employ only dimensionless parameters,[31] the results are representative for a class of polymeric materials in principle. One of these parameters is the noise scaling Ω, which was extensively discussed in previous publications.[32,33] In particular, the (discrete) noise amplitude is proportional to Ω^{-1}. We only repeat here that Ω can be interpreted as a size-expansion parameter in the Fokker–Planck theory[34] and comment shortly on the physical interpretation.

For an incompressible system, *i.e.* $\phi_A + \phi_B = 1$, Ω reflects the constant total number of coarse-grained monomers per cell of the computational grid. In other words, it appears rather naturally as a *scaling* due to the coarse-graining and discretization procedure. In particular, a higher Ω or, alternatively, more monomers per cell, gives rise to a reduced noise amplitude. One could understand this property from the fact that the relative composition fluctuations induced by adding monomers to a cell should depend on the (average) monomer density in the cell. The noise scaling is also lower bounded, since Langevin dynamics is unrealistic in the case of insufficient statistical averaging, *i.e.* for $\Omega = O(1)$. With no particular experimental system in mind, we used a standard value for Ω (see below). It can be shown that the fluctuation corrected interaction parameter χ_e of Fredrickson and Helfand[35] is very comparable to the Flory–Huggins χ at the microphase transition in the absence of fluctuations for this Ω.[33]

A noise term with standard noise scaling $\Omega = 10^2$ was added to eqn (1) at every time step for DDFT[31] and only white noise at $t = 0$ for CDS. Fig. 1 and 3 illustrate that the noise term in DDFT promotes the disassembly of misaligned structures and the formation of new nuclei in the disordered region, although its effect on the dynamic scattering behavior is small. We have also considered calculations in the absence of noise at $t = 0$ for CDS as well as for a reduced noise amplitude in DDFT ($\Omega = 10^3$). In these cases, the formation of new nuclei and the growth of existing ones were impeded, leading to very similar scattering intensities for both free energy models (not shown).

We also shortly comment on macroscopic separation into regions with small negative or positive angles relative to the EF in CDS (Fig. 3, $t = 800$). We conclude that these regions have grain boundaries with small interfacial tension, since they can be easily mixed when noise is added at each time step (Fig. 3, DDFT, $t = 800$).

In addition to starting from the well-defined structure shown in Fig. 3, we also considered the dynamics of a single structured nucleus in an electric field. Here, the selection of Ω is based on an alternative physical interpretation that involves the sampling distribution. One may view the stochastic term as a correction to the deterministic term in the Langevin model for diffusion. Since the deterministic part always leads to a reduced free energy,[33] the added noise provides global sampling, *i.e.* Boltzmann sampling in equilibrium, by facilitating barrier crossing on the free energy landscape. These barriers will generally be rather small, as the free energy differences for structures in soft materials are generally in the order of only a few k_BT. The probability of such events is directly related to the noise amplitude, and will thus decrease with increasing Ω. As discussed previously, and in more detail further on, the nucleation of new structures from the mixed phase is postponed by lowering Ω, which is a useful property for the analysis of growth rates of single nuclei.

This situation of a single nucleus relates to the scenario earlier described by Amundson *et al.*[36] where the ordered phase appears as several rather isolated nucleation centers, a lamellar structure within a sphere of varying radius R, that form due to composition fluctuations upon slow cooling from the disordered state. Here, all parameters are the same as in Fig. 3, except for the noise scaling Ω in DDFT (see below). Our starting point is the nucleus of $R = 16$ (in grid units) shown in Fig. 6a in an otherwise fully mixed ($\psi = 0$) surrounding. The initial concentration profile within the nucleus is sinusoidal perpendicular to the electric field direction, *i.e.* lamellae parallel to the EF, with a period derived from the lamellar distance in the final structure in Fig. 3. After a short equilibration for 10^2 time steps and a very low noise amplitude ($\Omega = 10^5$), to avoid fast destruction of the nucleus, the electric field is switched on at $t = 0$ (initially for $\Omega = 10^3$). The nucleus grows at first, with an increased growth rate in the direction perpendicular to the EF. Fluctuations in the mostly disordered surrounding start to grow in the direction of the EF ($t = 20$, Fig. 6a). The nucleus shows the characteristic, elongated shape that was already observed in Fig. 3. Very soon, the weakly phase segregated structure in the surroundings amplifies to form elongated structured nuclei as well ($t = 80$, Fig. 6a). Further unrestricted growth is impeded by merging at grain boundaries. This process is again accompanied by local (transient) disordering and nucleation of new seeds in places where two lamellae are misaligned, and we conclude that the system adopts the same pathway as in Fig. 3, including clusters merging at grain boundaries, defect migration and annihilation by merging with oppositely charged defects. Reducing the noise amplitude to $\Omega = 10^5$ from $t = 0$ (Fig. 6b) slows down the formation of new nuclei significantly. Also, the growth rate of the initial nucleus is slowed down, compare $t = 80$ in Fig. 6a and $t = 180$ in Fig. 6b, although the growth rate perpendicular to the EF is again larger. At $t = 580$ (Fig. 6b), in the yet largely disordered surroundings, multiple nuclei appear that are aligned with the EF. The order parameter in these nuclei is comparable to the one of $t = 20$ in Fig. 6a. Unrestricted growth has then led to a considerably larger single nucleus than for $\Omega = 10^3$. At later stages ($t = 780$), these nuclei

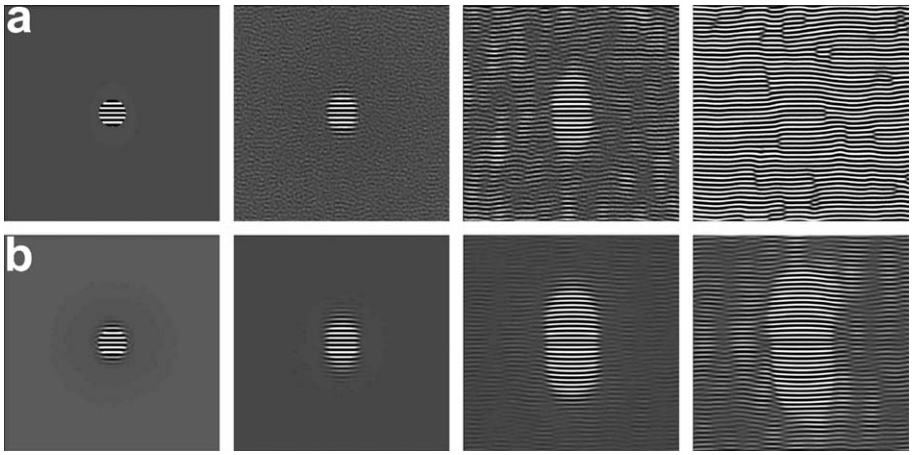

Fig. 6 Distinct stages of structure growth under an electric field ($\tilde{\alpha} = 0.2$) that was switched on at $t = 0$. The DDFT simulations started from a spherical lamellar nucleus with a radius $R = 16$ as seen in top left of (a). Two different scaling factors for the noise amplitude, $\Omega = 10^3$ (a) and $\Omega = 10^5$ (b), were used to study the influence of the noise on the growth rate. Corresponding time stages are (from left to right): (a) starting structure, 20, 80, 180 and (b) 20, 180, 580, 780. The electric field is applied along the horizontal direction.

grow both in size and order parameter in a similar fashion to the mechanism observed for $\Omega = 10^3$, although this process is again much slower. We can interpret these findings by referring to nucleation theory[36,37] that nuclei must have a critical size to withstand destruction due to composition fluctuations near ODT. Our results show that, when a small nucleus is formed, other nuclei appear almost immediately everywhere in the surroundings and then grow separately. Due to the close vicinity of nuclei and misalignment of the lamellae in these nuclei, they will be separated for some time, before merging, by a rather substantial grain boundary of disorder. As each of the nuclei is too small to survive, composition fluctuations will destroy them prior to this merging stage. On the other hand, going from order to disorder, the structure is isotropic on a larger scale and the few larger nuclei or clusters that remain after selective disordering can withstand these composition fluctuations and grow to merge, while smaller but transient nuclei are formed in the mixed region. This could explain the asymmetry in the behavior around ODT.

We conclude this analysis by letting $\Omega \rightarrow \infty$. Removing the noise term completely has the advantage that the growth of nuclei can be analyzed in the absence of new nuclei in the disordered region. We focus on the effect of the initial size and the electric field strength on the growth rate and final shape of the nuclei. In particular, the evolution of nuclei with different initial radii $R \in \{6, 12, 18\}$ was considered by varying the (constant) electric field strength $\tilde{\alpha} \in \{0.01,0.05,0.1,0.2,0.5\}$. The structures were first calibrated by slowly increasing the (dimensionless) time step to the desired value 0.2 at $t = 0$. Just like before, we performed the calculations for 4000 time steps ($t = 800$).

Fig. 8 shows the final structures for different $\tilde{\alpha}$. For a comparison, the structural evolution in the absence of an electric field, $\tilde{\alpha} = 0.0$, is shown in Fig. 7. We concentrate our analysis on the results obtained for $R = 12$, since we find that the structural evolution and final shape are independent of the seed, *i.e.* the size of the initial nucleus, but strongly depend on the electric field strength. We note that the growth rate itself may vary with the initial size of the nucleus, but we analyze these dependencies later.

First, we consider structural evolution in the absence of an applied electric field, Fig. 7. As may be expected, the boundary between the mixed phase and the structured, lamellar seed is unfavorable for both entropic and enthalpic reasons. The associated thermodynamic driving force is clearly large enough for the lamellae to eventually *curve* around the nucleus and close up into ellipses at the initial plane of symmetry. The elliptical shape and the overall compressed onion-like structure stems from geometric constraints, as these newly formed rings have to adapt to both the well-defined lamellar orientation in the seed and, in order to close up, to integer multiples of the lamellar distance. Closing up is accompanied by considerable local curvature in the zone where lamellae meet, resulting in rearrangement *via* (partial) melting in this zone. Closer to the seed, however, the high curvature cannot be relieved and the associated stress gives rise to zones where phase segregation is persistently suppressed (see $t = 800$). The radial distribution of these suppression zones is reminiscent of acoustic scattering by a slit. Nevertheless, the structural growth is overall surprisingly isotropic and new layers increasingly adapt a circular shape with constant curvature, as in the final structure in Fig. 7.

Comparing Fig. 7 and 8, we identify several competing factors responsible for the final shape of the nucleus: the lamellar tendency to curve around the seed, electric-field-induced growth parallel to the electric field and suppression of misaligned structures. The lamellar break-up by undulations that precedes mixing in mechanisms A and A′ originates from an imbalance between the surface tension and the ponderomotive force, and thus depends on the temperature, the angle to the electric field direction and the electric field strength $\tilde{\alpha}$. For the considered $\varepsilon_{AB} = 4.6$, or equivalent, $\tau = 0.3$ in CDS, we can use the diagrams in the previous study of Pinna *et al.*[21] to estimate the electric field strength required for, in this case, the *suppression* of misaligned structure. A transition between mechanisms A and A′ was found at $\tilde{\alpha} \approx 0.04$, where the response of misaligned structure to the applied electric field switches from partial mixing (at defects) to almost complete mixing. In the remainder, orientations and alignment are discussed with respect to the electric field direction, *i.e.* the horizontal direction in Fig. 8.

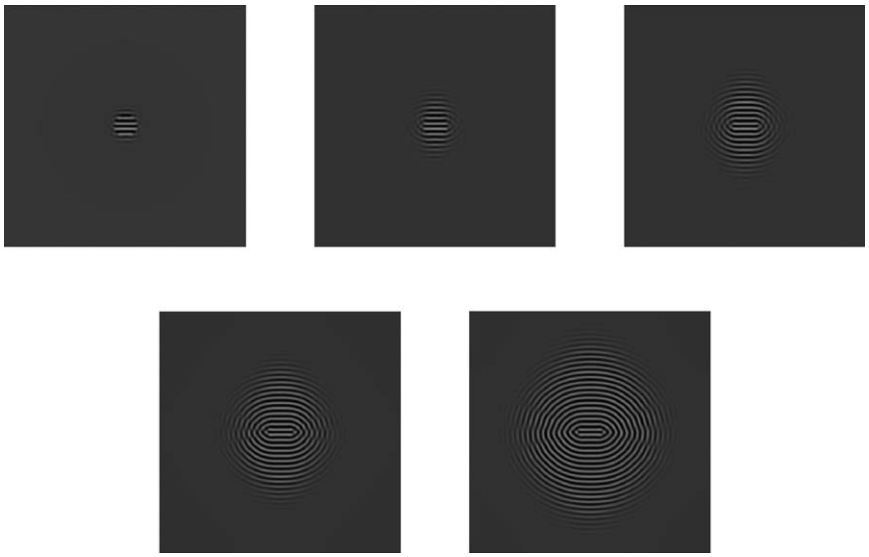

Fig. 7 Structural evolution in the absence of an electric field and noise. The DDFT calculations started from a spherical lamellar seed with a radius $R = 12$. Corresponding time stages are (from left to right, top to bottom): starting structure, 200, 400, 600 and 800. The electric field is applied along the horizontal direction.

With increasing $\tilde{\alpha}$, Fig. 8, we distinguish three different final nuclei shapes: an onion, a dumbbell and an ellipse. The transition from an onion to a dumbbell shape is found between $\tilde{\alpha} = 0.01$ and 0.05, in agreement with the transition value $\tilde{\alpha} \approx 0.04$ of the previous study. We note that the growth rate perpendicular to the electric field is apparently not affected by the electric field, which is important for the observed shapes and will be considered in more detail later on. For the weakest electric field, $\tilde{\alpha} = 0.01$, the field is clearly not strong enough to suppress the formation of misaligned structure, although the growth of the onion in the parallel direction is slightly impeded compared to $\tilde{\alpha} = 0.0$. This observation shows once again that lamellae under a *large* angle to the field are sensitive to rather weak electric fields close to ODT. For an increased field strength, $\tilde{\alpha} = 0.05$, only the onset of lamellar curving is observed. Further curving towards the initial plane of symmetry is prevented by the electric field, which suppresses the formation of lamellae above a certain $\tilde{\alpha}$-dependent threshold angle. Meanwhile, the lamellae in the seed also grow in the parallel direction, but the rate is rather small for $\tilde{\alpha} = 0.05$. The result of all these contributions is the typical dumbbell shape. With further increased $\tilde{\alpha}$, lamellar curving is increasingly suppressed and the growth rate of lamellae along the field direction rises. In combination, they result in an almost straight perpendicular structured interface for $\tilde{\alpha} = 0.1$ and an increasingly elliptic shape for larger $\tilde{\alpha}$. An elliptic shape with only straight lamellae is found for the largest field strength considered, $\tilde{\alpha} = 0.5$. One could conclude that isotropic growth is recovered somewhere in the range $\tilde{\alpha} > 0.5$. However, we repeat that

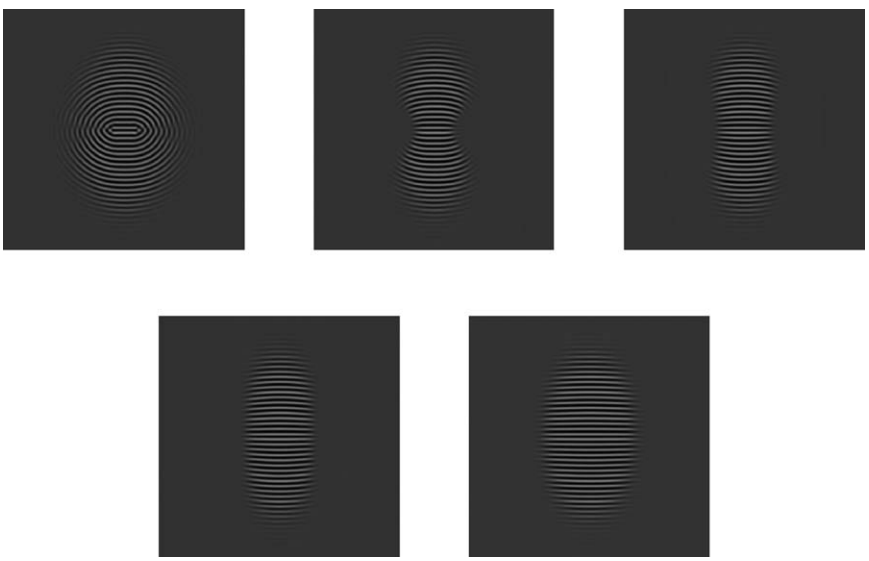

Fig. 8 Final stages ($t = 800$) of structure growth under an electric field that was switched on at $t = 0$. The DDFT calculations started from a spherical lamellar nucleus with a radius $R = 12$ and no noise was added. Corresponding field strengths $\tilde{\alpha}$ are (left to right, top to bottom): 0.01, 0.05, 0.1, 0.2 and 0.5. The electric field is applied along the horizontal direction.

$\tilde{\alpha} = 0.2$ can be related to an already large experimental field value $E_0 \approx 10$ V/μm.

Finally, we perform a quantitative analysis of growth rates. For the analysis, we determined the size and shape of the structured nucleus by thresholding the order parameter field, followed by a coarsening procedure. This procedure brings along a smearing of the boundaries, but does not seriously affect the growth rates (see below). A few significant results of this procedure, enabling a clearer view of the different shapes with increasing electric field strength ($t = 800$), are shown in Fig. 9. Assuming symmetric growth and using the center (x_m, y_m) of the nucleus as a reference, we focus on the growth in the perpendicular, $a(t) = |x_b - x_m|$, and parallel direction, $b(t) = |y_b - y_m|$, where x_b and y_b are the positions of the boundary of the nucleus at time t, obtained from projection onto the two Cartesian axes. In addition, we determined the size $b_{min}(t) = |y_{min} - y_m|$ of the 'waist', *i.e.* parallel to the field in the center of the nucleus, where y_{min} is the position of the boundary at $x = x_m$. A schematic illustration of the way that these values are determined at each time step, after the coarsening procedure, is shown in Fig. 10. The shape in Fig. 10 is a generic dumbbell, and we note that all nuclei shapes are considered accordingly. For the dumbbell shape, $b_{min} < b$, while for the elliptical shape, $b_{min} = b$. Determining the shape and size of the onion is a subtle issue, as the order field in the outer layers is rather low and sensitive to thresholding. For completely isotropic growth $a(t) = b(t) = b_{min}(t)$. The resulting curves where fitted by a quadratic polynomial

$$p(t) = c_0 + c_1 t + c_2 t^2. \quad (5)$$

In Fig. 11, we only plot the coefficient c_1 of the linear term, which we denote as the growth rate r_i ($i \in \{a, b, b_{min}\}$), for different initial radii R and field strengths $\tilde{\alpha}$, noting that $c_2 \ll c_1$ in all cases.

Using Fig. 11, we analyze the growth rates for $R = 6$ (a, top/left), $R = 12$ (b, top/right) and $R = 18$ (c, bottom/left). We have added data for $R = 12$ (d, bottom/right) where a noise term according to the fluctuation-dissipation theorem, with $\Omega = 10^5$, was added to (1) at each time step. In the latter case, growth rates were calculated using only the first part ($t \leq 200$) of the structural evolution. Comparing the right panel, $R = 12$, in the absence and presence of noise, it is clear that noise leads to growth rates that are all considerably reduced (compare ○, □ and ◇ in Fig. 11b and d). Since we have previously concluded that an increased Ω gives rise to impeded growth rates, this finding seems contradictory, but it only shows that the thermodynamic driving forces are indeed small close to ODT. The very similar trends of the three different rates, in the absence and presence of noise, give us enough confidence to conclude that we can indeed neglect the effect of noise for this analysis.

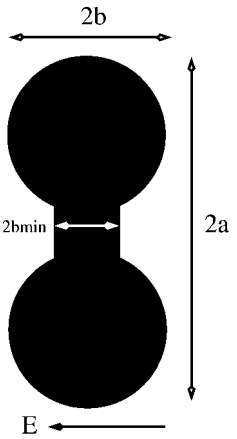

Fig. 10 Schematic illustration, showing how a, b and b_{min} are determined for a given shape. This example is for a dumbbell; values for other shapes are determined in exactly the same way.

Concentrating first on r_a (○), the growth rate in the perpendicular direction, we see that it is almost constant, *i.e.* independent of the electric field strength, for each individual value of R. Only for the smallest seed, $R = 6$, the absolute value of this r_a is considerably smaller than for the other, larger seeds, compare Fig. 11a (○) with Fig. 11b–c (○). In the absence of an electric field, the growth of the onion shape is also less isotropic for $R = 6$ than for $R = 12$, which can be seen from comparing r_a (○) and r_b (□) in both Fig. 11a and b for $\tilde{\alpha} = 0.0$, noting that for isotropic growth $r_a = r_b$. The origin of this size dependence is unclear, but one should keep in mind that both the number of lamellae and the boundary area for $R = 6$ are considerably smaller than for the larger seeds. Likewise, one may conclude that the thermodynamic driving force for curving around the seed is decreased. This size dependence is absent for larger seeds, compare the graphs for $R \in \{12, 18\}$. We find that the *trends* for r_a, r_b and $r_{b_{min}}$ *versus* the electric field strength are very similar for all considered R.

We use this observation to distill generic features and consider the rates associated with the maximal and minimal structure size in the direction parallel to the electric field: r_b (□) and $r_{b_{min}}$ (◇). For $0 \leq \tilde{\alpha} < 0.2$, we find that $r_{b_{min}} < r_b$, indicative of a dumbbell shape, and for $\tilde{\alpha} \geq 0.2$, we find $r_{b_{min}} = r_b$, indicative of an ellipse. With the exception of the weakest electric field strengths, $\tilde{\alpha} =$ 0.0–0.01, for which we find a onion shape, the curve for $r_{b_{min}}$ (◇), the growth rate for the 'waist' of the nucleus, has a characteristic logarithmic shape. This shows that the growth rate in the direction parallel to the field indeed increases (logarithmically) with increased field strength. Concentrating on the curve for r_b

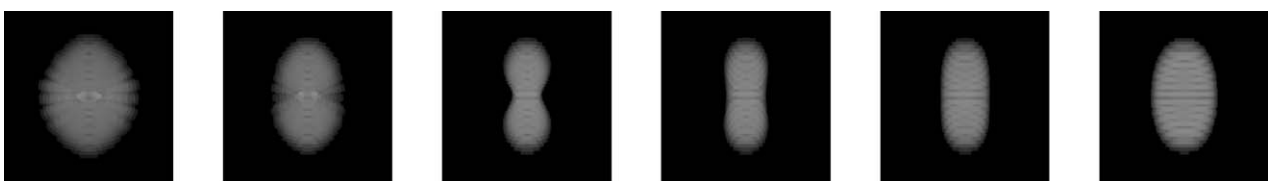

Fig. 9 The thresholded and smeared field, input for the analysis of the growth rates, for the structures that are shown in Fig. 7 ($t = 800$) and Fig. 8. Corresponding field strengths $\tilde{\alpha}$, from left to right, are: 0.0, 0.01, 0.05, 0.1, 0.2 and 0.5. The electric field is applied along the horizontal direction.

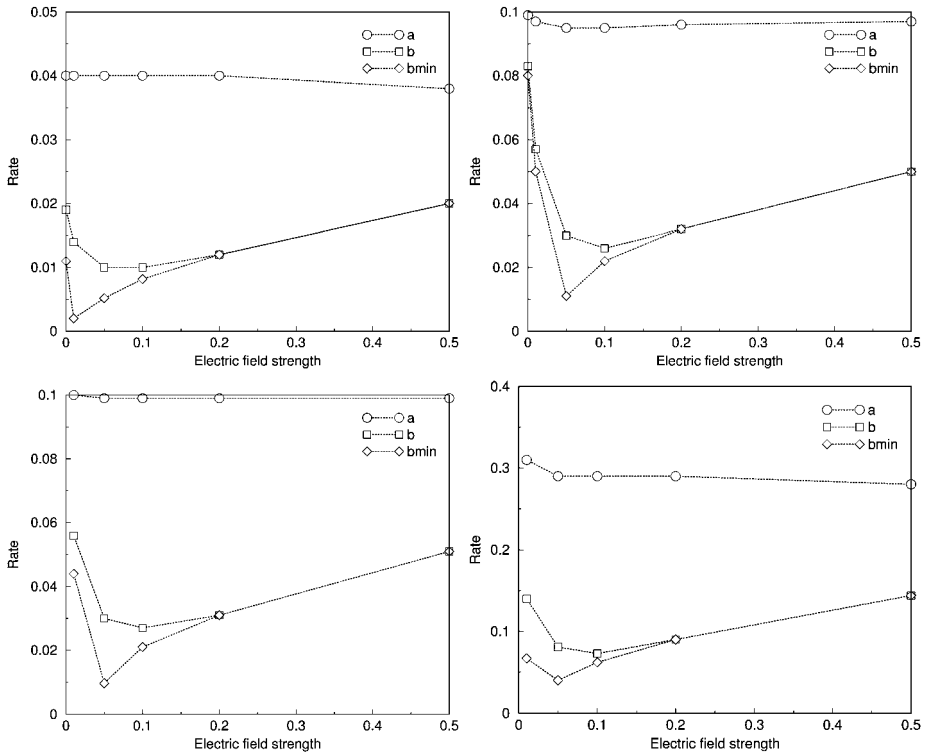

Fig. 11 Growth rates r_a, r_b and r_{bmin} *versus* electric field strength $\tilde{\alpha}$, resulting from a quadratic fit of the nucleus size in the perpendicular (a) and parallel (b) direction as well as the size in the centre region of the nucleus in the parallel direction (b_{min}). The coefficient of the linear term in the fit to the polynomial $p(t) = c_0 + c_1 t + c_2 t^2$ is displayed and the radius of the seed R varied. Top/left: $R = 6$ (a) and top/right: $R = 12$ (b). Bottom/left: $R = 18$ (c). The bottom/right (d) graph shows the growth rates for $R = 12$ when noise with $\Omega = 10^5$ is added at each time step.

(□), we find that it experiences a local maximum for $\tilde{\alpha} = 0.0$ and a minimum for $\tilde{\alpha} = 0.1$, showing that an increased $\tilde{\alpha}$ gives rise to decreased curvature of lamellae in the nucleus. The balance of these different contributions gives rise to the final shape, either an onion (small $\tilde{\alpha}$), a dumbbell (intermediate $\tilde{\alpha}$) or an ellipse (large $\tilde{\alpha}$). We conclude that all previous qualitative observations are supported by this quantitative analysis. Since we linked the final shape to the underlying mechanisms, the conclusions can be easily extrapolated, for instance to systems with higher ε_{AB} and/or a different seed structure.

As a final comment, we note that (1) does not account for hydrodynamic effects. A combination of experiments and a numerical investigation based on Navier–Stokes and a Brazovskii free energy functional[38] suggests that structured nuclei can rotate as a whole to align to the field direction, in addition to the pre-alignment, upon a quench just below ODT. As both the parameters in the model and the mechanism of grain rotation itself are not fully clarified, it is hard to make a detailed comparison to this study. We performed additional calculations (results not shown here) for $\tilde{\alpha} = 0.05$ and $\tilde{\alpha} = 0.5$, starting with a seed like in Fig. 6a that is rotated by 45°. For both field strengths, the lamellae are found to rotate by *melting*. The surviving structure, lamellar fragments near the boundary of the seed, form two new seeds with aligned lamellae. For the weakest field, the melting process is fairly slow and only partial, and coincides with the growth of new seeds. For the strongest field, melting is instantaneous and almost complete. Further growth shows an electric field strength signature that is very similar to the one discussed before. On the basis of these observations, and the fact that the viscosity in these systems is generally rather high, we argue that grain rotation may be involved, but that the mechanisms discussed here are most important.

4 Conclusions

We considered the detailed microscopic response of a defected, phase-separated structure, which is isotropic on a larger scale, to an externally applied electric field close to ODT by two different methods, one being molecular (DDFT) and the other phenomenological (CDS), and found that the new mechanism of selective melting earlier observed by CDS is one-to-one reproduced by DDFT. We considered and analyzed in detail the fundamentals of this mechanism. The results presented here have a general character and may serve as a stepping stone for understanding dynamic response pathways due to other kinds of deformation, such as mechanical stress or shear. We also considered the growth of a single structured nucleus in an applied electric field by DDFT. The noise term in Langevin dynamics, which is usually added and always in agreement with the fluctuation-dissipation theorem, can be used to concentrate on different aspects of the phenomena. By suppressing the formation of new nuclei, *i.e.* no noise term, we were able to determine three distinct shapes for the growing nucleus—an onion, a dumbbell and an ellipse—and analyze their origin. We found that this shape is determined by the electric field strength. We also considered the realistic situation where new nuclei form in the mixed region, *i.e.* the standard noise term, and found that nuclei are usually separated by a substantial (transient) grain boundary of disorder.

We discussed how this restricted growth provides a possible explanation for the heavily debated, experimentally observed asymmetry of the ODT-dependence on the electric field strength. Nevertheless, further research is required and left for future publications. The reorientation mechanism is most effective for values of $\chi_{AB}N$ that are slightly higher than $(\chi_{AB}N)^{ODT}$, at which the system is slightly demixed and the balance between surface tension and the ponderomotive force is optimal.

5 Acknowledgements

Simulations were performed at UCLan High Performance Computing Facilities (Preston) and the Huygens supercomputer at SARA (Amsterdam). The authors acknowledge support by the NanoSci E+ ERA-NET project MEMORY. GJAS acknowledges support by a Supercomputer time grant from the Stichting Nationale Computerfaciliteiten (NCF) and MP by Accelrys Ltd. through EPSRC CNA research studentship.

References

1 A. Zvelindovsky, *Nanostructured Soft Matter*, Springer, 2007.
2 S. B. Darling, *Prog. Polym. Sci.*, 2007, **32**, 1152.
3 K. Amundson, E. Helfand, X. Quan, S. D. Hudson and S. D. Smith, *Macromolecules*, 1994, **27**, 6559.
4 T. Xu, C. J. Hawker and T. P. Russell, *Macromolecules*, 2003, **36**, 6178.
5 J. Y. Wang, W. Chen and T. P. Russell, *Macromolecules*, 2008, **41**, 7227.
6 K. Schmidt, H. G. Schoberth, M. Ruppel, H. Zettl, H. Hänsel, T. Weiss, V. Urban, G. Krausch and A. Böker, *Nat. Mater.*, 2008, **7**, 142.
7 V. Olszowka, M. Hund, V. Kuntermann, S. Scherdel, L. Tsarkova and A. Böker, *ACS Nano*, 2009, **3**, 1091.
8 E. J. W. Crossland, S. Ludwigs, M. A. Hillmyer and U. Steiner, *Soft Matter*, 2010, **6**, 670.
9 Y. Tsori and D. Andelman, *Macromolecules*, 2002, **35**, 5161.
10 M. Matsen, *Phys. Rev. Lett.*, 2005, **95**, 258302.
11 C.-Y. Lin, M. Schick and D. Andelman, *Macromolecules*, 2005, **38**, 5766.
12 C.-Y. Lin and M. Schick, *J. Chem. Phys.*, 2006, **125**, 034902.
13 I. Gunkel, S. Stepanow, T. Thurn-Albrecht and S. Trimper, *Macromolecules*, 2007, **40**, 2186.
14 A. Onuki, *Phase Transition Dynamics*, Cambridge University Press, 2007.
15 A. Onuki and J. Fukuda, *Macromolecules*, 1995, **28**, 8788.
16 M. W. Matsen, *Soft Matter*, 2006, **2**, 1048.
17 J. Fukuda and A. Onuki, *J. Phys. II*, 1995, **5**, 1107.
18 A. Böker, H. Elbs, H. Hänsel, A. Knoll, S. Ludwigs, H. Zettl, V. Urban, V. Abetz, A. H. E. Müller and G. Krausch, *Phys. Rev. Lett.*, 2002, **89**, 135502.
19 A. V. Zvelindovsky and G. J. A. Sevink, *Phys. Rev. Lett.*, 2003, **90**, 049601.
20 A. Böker, V. Abetz and G. Krausch, *Phys. Rev. Lett.*, 2003, **90**, 049602.
21 M. Pinna, L. Schreier and A. V. Zvelindovsky, *Soft Matter*, 2009, **5**, 970.
22 J. DeRouchey, T. Thurn-Albrecht, T. Russell and R. Kolb, *Macromolecules*, 2004, **37**, 2538.
23 H. Schoberth, K. Schmidt, S.K.A. and A. Böker, *Macromolecules*, 2009, **42**, 3433.
24 C. Lin, *Macromolecules*, 2005, **38**, 5766.
25 M. Pinna, A. V. Zvelindovsky, S. Todd and G. Goldbeck-Wood, *J. Chem. Phys.*, 2006, **125**, 154905.
26 K. S. Lyakhova, A. V. Zvelindosky and G. J. A. Sevink, *Macromolecules*, 2006, **39**, 3024.
27 B. C. Berry, A. W. Bosse, J. F. Douglas, R. L. Jones and A. Karim, *Nano Lett.*, 2007, **7**, 2789.
28 N. Sakamoto and T. Hashimoto, *Macromolecules*, 1998, **31**, 3815.
29 A. Knoll, A. Horvat, K. S. Lyakhova, G. Krausch, G. J. A. Sevink, A. V. Zvelindovsky and R. Magerle, *Phys. Rev. Lett.*, 2002, **89**, 035501.
30 A. Knoll, K. S. Lyakhova, A. Horvat, G. Krausch, G. J. A. Sevink, A. V. Zvelindovsky and R. Magerle, *Nat. Mater.*, 2004, **3**, 886.
31 B. A. C. van Vlimmeren, N. M. Maurits, A. V. Zvelindovsky, G. J. A. Sevink and J. G. E. M. Fraaije, *Macromolecules*, 1999, **32**, 646.
32 B. A. C. van Vlimmeren and J. G. E. M. Fraaije, *Comput. Phys. Commun.*, 1996, **99**, 21.
33 J. G. E. M. Fraaije, B. A. C. van Vlimmeren, N. M. Maurits, M. Postma, O. A. Evers, C. Hoffmann, P. Altevogt and G. Goldbeck-Wood, *J. Chem. Phys.*, 1997, **106**, 4260.
34 N. van Kampen, *Stochastic Processes in Physics and Chemistry*, North-Holland, Amsterdam, 1992.
35 G. H. Fredrickson and E. Helfand, *J. Chem. Phys.*, 1987, **87**, 697.
36 K. Amundson, E. Helfand, D. Davis, X. Quan and P.S.S., *Macromolecules*, 1991, **42**, 6546.
37 G. Fredrickson and K. Binder, *J. Chem. Phys.*, 1989, **91**, 7265.
38 T. Taniguchi, R. Uchino, M. Sugimoto and K. Koyama, in: *AIP Conference Proceedings 982*, 2008, p. 482.

